INTERNATIONAL JOURNAL OF HYDROGEN ENERGY 48 (2023) 14337–14347

Available online at www.sciencedirect.com

ScienceDirect

journal homepage: www.elsevier.com/locate/he

Peculiarities of the absorption and desorption of hydrogen by opal matrices

*K.P. Meletov**, *V.S. Efimchenko*, *M.A. Korotkova*, *V.M. Masalov*, *N.S. Sukhinina*, *G.A. Emel'chenko*

Osipyan Institute of Solid State Physics RAS, Chernogolovka, Moscow Region, 142432 Russia

HIGHLIGHTS

- Intense absorption of hydrogen occurs in synthetic opal matrices at high pressure.
- The H_2 molecules are embedded directly into silica spheres and voids between them.
- The hydrogen content in opal structures decreases exponentially under long-term heating.
- Under the heating, the hydrogen losses occur equally from both localizations.
- The activation energy E_A of hydrogen desorption is (162 ± 13) meV.

GRAPHICAL ABSTRACT

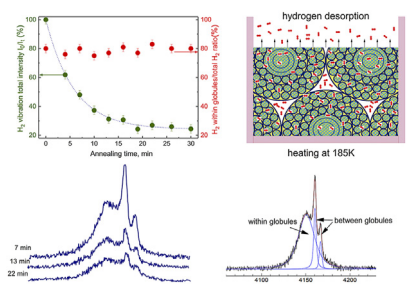

ARTICLE INFO

Article history:
Received 10 October 2022
Received in revised form
12 December 2022
Accepted 24 December 2022
Available online 12 January 2023

Keywords:
Synthetic opal matrices
Hydrogen storage
High pressure
Raman scattering

ABSTRACT

The absorption and desorption of hydrogen at high pressure and temperature by opal matrices formed by amorphous silica spheres with a diameter of 0.235 and 1.6 μm have been studied. The Raman spectra of hydrogen-saturated opal matrices measured at a temperature of 80 K and ambient pressure show that hydrogen molecules are adsorbed in two different ways, directly into silica spheres and mesopores between them. The kinetics of hydrogen desorption was studied *in-situ* from a change in the relative intensity of rotational modes in the Raman spectra under annealing at 163–213 K. The hydrogen content decreases exponentially under isothermal heating, while the exponential decay time constant τ increases with a decreasing temperature showing the activation nature of desorption. The data for various temperatures are well described by the Arrhenius dependence $\tau(T) = A \times \exp(E_A/k_BT)$ with the activation energy E_A=(162 ± 13) meV and time constant A= (1.8 ± 0.5) × 10^{-2} s.

© 2022 Hydrogen Energy Publications LLC. Published by Elsevier Ltd. All rights reserved.

* *Corresponding author.*
E-mail address: mele@issp.ac.ru (K.P. Meletov).
https://doi.org/10.1016/j.ijhydene.2022.12.297
0360-3199/© 2022 Hydrogen Energy Publications LLC. Published by Elsevier Ltd. All rights reserved.

Introduction

The intense absorption of hydrogen in condensed media was observed in various materials: metals and alloys, clathrates of various gases, ice hydrates, carbon structures, and, finally, silicate glasses of various compositions [1–5]. The search for new solid materials, namely, hydrogen storage containers is a relevant task of green energy since they are necessary for the safe storage of hydrogen at a higher specific density compared to the storage of liquefied gas in metal tanks [6,7]. The amount of absorbed hydrogen and the prevalence of the employed material, as well as the manufacturability of the processes of hydrogen saturation/release, are key factors in evaluating the possibility of the practical application of the containers being developed. In this regard, various silicate glasses [5,8,9], as well as finely dispersed structures based on them, are of certain interest. In particular, hollow and filled silica spheres of micron and submicron sizes are interesting materials for possible use as hydrogen storage containers [10,11].

In optically transparent silicate glasses, hydrogen is absorbed in the molecular form [5]. This provides an opportunity to use Raman spectroscopy to identify absorbed molecular hydrogen and estimate its amount, as well as to study the properties of hydrogen-saturated silicate glasses under various conditions. Even slight absorption of hydrogen by silicate glass is manifested in the Raman spectra in the form of vibration and rotational modes of hydrogen molecules along with phonon modes of silicate glass. When silicate glasses are saturated with hydrogen under the conditions of high pressure up to 7.5 GPa and at a temperature of 250 °C, the hydrogen molar content $X = H_2/SiO_2$ can reach 0.7. This leads to significant changes in the phonon spectrum of silicate glasses, which are reliably recorded in the Raman spectra at a temperature near the boiling point of liquid nitrogen [5,8,9,12]. Under ambient conditions, hydrogen-saturated silicate glasses rapidly lose adsorbed hydrogen. To reduce these losses, after synthesis the samples are quenched and stored in liquid nitrogen. The hot extraction method [13] is usually used to determine the total amount of absorbed hydrogen. At the same time, Raman spectroscopy allows not only establishing the fact of the absorption of molecular hydrogen but also estimating its amount in the material as well as studying the losses under the heating of samples in real-time mode. By using *in-situ* Raman measurements, for the first time, the kinetics of hydrogen losses at various temperatures was investigated from a change in the relative intensity of the rotational phonon modes of hydrogen in the Raman spectra of hydrogenated silicate glass, the activation nature of the process was established, and the activation energy of hydrogen desorption was determined [14].

In this paper, we present the results of the study of hydrogen absorption by synthetic opal matrices of two types: those formed by silica spheres with a diameter of 235 nm (OM-235) and 1600 nm (OM-1600). It was found that the OM-235 and OM-1600 matrices could be saturated with hydrogen to a molar ratio of $0.8H_2/SiO_2$ at 7.5 GPa and 140 °C, the properties of the obtained samples being completely identical in both cases. The Raman spectra of hydrogenated $0.8H_2$/OM-1600 opal matrices were measured at various temperatures from 80 to 213 K and ambient pressure. It is shown that hydrogen molecules are embedded into both the voids of the amorphous silica microspheres and mesopores between them. This leads to the emergence of relatively narrow and rather broad bands in the range of Raman frequencies corresponding to the rotational and vibration modes of a hydrogen molecule. As was shown earlier, the broad bands correspond to hydrogen absorbed directly by amorphous silica [14], while the narrow bands are most likely related to hydrogen gas located in the mesopores between the silica microspheres. The hydrogen losses under the isothermal heating of $0.8H_2$/OM-1600 samples were studied *in-situ* by Raman measurements of the hydrogen vibration mode. It was found that hydrogen released in a parallel way from both the silica microspheres and the mesopores between them at the same rate. Similarly, a change in the relative intensity of the hydrogen rotational modes was studied, and data on the kinetics of hydrogen desorption were obtained. Raman measurements in the temperature range of 163–213 K showed that the hydrogen content in hydrogenated opal matrices decreased exponentially with heating time, while the time constant of the exponential decay τ decreased with an increase in the temperature. The data obtained at various temperatures indicate the activation nature of hydrogen desorption and are well described by the Arrhenius dependence $\tau(T) = A \times \exp(E_A/k_BT)$, where T is the temperature, k_B is the Boltzmann constant, E_A is the activation energy that is (162 ± 13) meV, and A is the time constant that is $(1.8 \pm 0.5) \times 10^{-2}$ s.

Experimental

Spherical silica particles with a diameter of 0.235 ± 0.01 μm and 1.6 ± 0.06 μm were obtained by the modified Stöber-Fink-Bohn (SFB) method [15] by the hydrolysis of tetraethoxysilane (TEOS) in a water-alcohol solution in the presence of ammonium hydroxide as a catalyst (50% vol. ethanol, 1.0 M ammonia). For the controlled synthesis of particles with given sizes, the multi-stage growth method was used. For this purpose, part of the suspension obtained at the previous synthesis stage was diluted in the corresponding volume of a water-alcohol-ammonia mixture of the same composition, and additional portions of TEOS were introduced into the reaction mixture. The calculated amount of single-loaded TEOS excluded the possibility of the nucleation of particles of the second generation and the emergence of the bimodal size distribution of the particles. The opal matrices were formed from the obtained silica spheres by particle sedimentation followed by drying of the precipitates at 150 °C and annealing at 600 °C for 4 h. Drying at 150 °C enabled removing physical water from the opal matrix structure [16], and annealing at 600 °C allowed removing chemically combined water and residues of organic substances from the matrix. At the same time, the porosity of the structure changed little, and its strength increased significantly.

The obtained silica spheres with a diameter of 0.235 μm and 1.6 μm differed in their internal structure [17,18]. Spheres with a diameter of 0.235 μm consisted of "primary" particles of molecularly bounded silica with a diameter of 5–7 nm and a

density of 2.22 g/cm^3. Under multi-stage synthesis of spherical particles, each growth stage was completed by the formation of a dense layer. This layer consisted of packed "primary" particles and an additional amount of molecular silica that filled the space between them. Thus, the internal structure of OM-235 particles with a diameter of 0.235 μm was a system of close-packed "primary" particles alternating with dense concentric layers (according to the number of growth stages). The internal structure of the particles contained pores with characteristic sizes of 2–3 nm and 1–1.5 nm (in a quantitative ratio of 1:2) and channels between them with a diameter of less than 1 nm. Dense concentric layers also had a system of pores that made the layers permeable to water molecules (a kinematic diameter of 0.265 nm) and impermeable to "larger-molecular" liquids (methanol, ethanol, etc.) [19]. Spheres with a diameter of 1.6 μm had a "nucleus" with a diameter of ~0.35 μm and an internal structure similar to that described above for particles with a diameter of 0.235 μm. The nucleus was surrounded by the shells of layers of "secondary" spherical particles with a diameter of about 20–40 nm, the internal structure of which was identical to the nucleus structure. Each concentric layer of "secondary" particles was covered with a dense spherical shell of a mixture of "primary" particles and molecular silica. Particles with a diameter of 1.6 μm had an additional system of pores between "secondary" spheres in the shells with sizes of 8–16 nm and 4–9 nm and channels between them with a characteristic diameter of 3–6 nm. The internal structure of the two types of particles is shown schematically in Fig. 1.

The synthetic opal matrices were saturated with hydrogen in a toroid-type high-pressure apparatus [20] using AlH_3 [21] or NH_3BH_3 [22] as internal hydrogen sources. The high-pressure cell was made of Teflon, and a Pd foil inside it separated the hydrogen source from the opal matrix. To release hydrogen, its AlH_3 (NH_3BH_3) sources were decomposed at P = 1.5 GPa and T = 250 °C. Then, the temperature was decreased to T = 140 °C, the hydrogen pressure was increased to P = 7.5 GPa, and the samples were kept under these conditions for 24 h. After this procedure, the samples were quenched by rapid cooling to liquid nitrogen temperature to exclude hydrogen losses under the subsequent release of pressure to the normal one. The samples were stored in a Dewar vessel with liquid nitrogen. The molar ratio X = H_2/SiO_2 of the obtained samples was determined with an accuracy of ~3% by hot extraction of the absorbed hydrogen into a pre-evacuated quartz ampoule [13]. The sample was placed from a liquid nitrogen bath into an open copper container, while the latter was placed in the quartz ampoule that was cooled from outside by liquid nitrogen. The ampoule was attached to a vacuum system with the calibrated volume, the system was pumped out to a pressure of 0.136 Pa, and then the ampoule was heated at a rate of 20 K/min, with simultaneous measurement of the pressure of the gas released during heating to 600–650 °C. The sample mass was determined by weighing after the measurements, while the mass of extracted hydrogen was calculated using the data on the ampoule volume and gas pressure.

The regularities of hydrogen desorption at a temperatures above the boiling point of liquid nitrogen were studied *in-situ* from a change in the relative intensities of hydrogen phonon modes in the Raman spectra of hydrogen-saturated opal matrices. The Raman spectra were recorded in back-scattering geometry at a temperature close to that of liquid nitrogen in the spectral range of 150–4400 cm^{-1} using a setup comprised of an Acton SpectraPro-2500i spectrograph and a CCD Pixis2K detector cooled down to −70 °C (2048 × 512 pixels, a size of 13 μm). To excite the Raman spectra, a stabilized single-mode YAG laser with a radiation wavelength of 532 nm was used. The laser beam was focused on the sample in a ~2-μm-diameter excitation spot by an Olympus BX51 microscope and an Olympus × 50 objective with a working distance of 12 mm. The spectral resolution of the setup was ~3 cm^{-1}, and the laser radiation line was suppressed by an edge filter with a bandwidth of ~100 cm^{-1} and the optical density OD = 6. The laser radiation intensity in the excitation spot was about 6 mW. The measurements of the Raman spectra were performed at various temperatures using a home-made nitrogen cryostat with cold loading of samples, which permitted placing samples with absorbed hydrogen on the cold table of the cryostat directly from liquid nitrogen without intermediate warming. The temperature control system comprised of a temperature controller and a resistive heater on the heat exchanger of the cold table enabled maintaining the temperature of the samples in the range of 80–250 K with an accuracy of about ±0.4 K [23].

Results and discussion

Fig. 2 depicts the Raman spectra of the samples of hydrogen-saturated $0.6H_2/SiO_2$ silicate glass (open circles) and hydrogen-saturated opal matrices $0.8H_2$/OM-1600 (closed circles), in the energy range of 255–4260 cm^{-1} at ~80 K and normal pressure. The solid line in the figure shows the Raman spectrum of gaseous hydrogen at a pressure of ~0.5 MPa and at room temperature. The latter spectrum contains very narrow lines corresponding to the characteristic phonon modes of a diatomic hydrogen molecule. In the low-energy region, these are $S_0(0)$ and $S_0(1)$ rotational modes with frequencies of 354 cm^{-1} and 587 cm^{-1} corresponding to para- and ortho-hydrogen, respectively. In the high-energy region, these are $Q_1(0)$ and $Q_1(1)$ H–H stretching vibration modes with frequencies of 4162.5 cm^{-1} and 4155.5 cm^{-1}, also corresponding to para- and ortho-hydrogen [24,25].

The phonon spectrum of a free hydrogen molecule is known to consist of rotational modes associated with the rotation of a diatomic molecule and stretching vibration modes resulting from the vibrations of hydrogen atoms along the H–H bond. The energy of rotational phonon modes is determined by the formula:

$$E = B_0 \times J \times (J+1) \quad (1)$$

where $B_0 = h/(8\pi^2 Ic)$ is the rotational constant, J = 0, 1, 2, …is the rotational quantum number, $I = \mu R^2$ is the moment of inertia of a diatomic molecule (μ is the reduced mass, and R is the distance between atomic nuclei), h is the Planck constant, and c is the speed of light. The energy of stretching vibrations is determined by the formula:

$$E = (n+1/2) \times h\nu \quad (2)$$

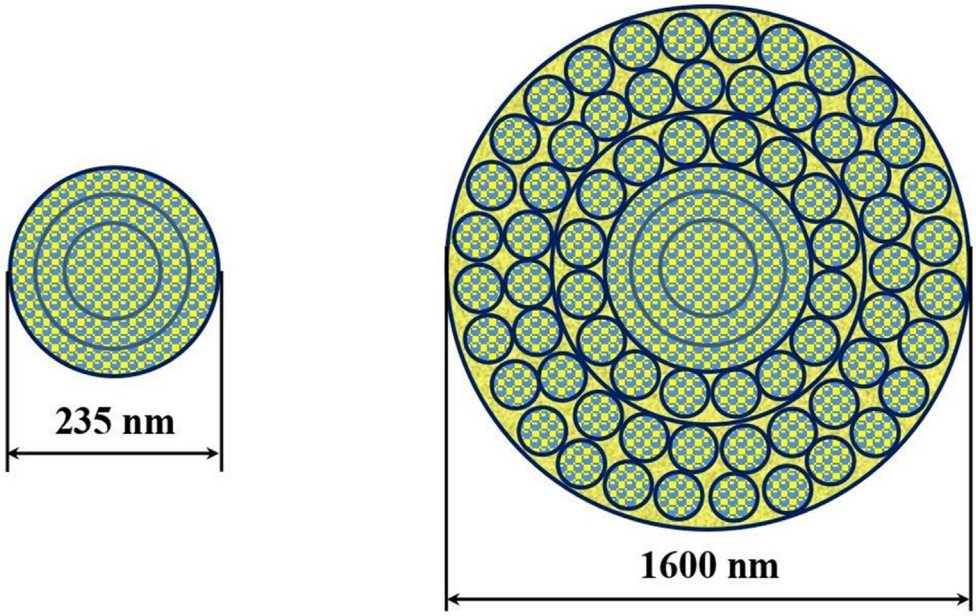

Fig. 1 – Schematic representation of the internal structure of silica spheres of various sizes obtained by the modified SFB method. The body of the silica spheres and bounding spherical silica shells are marked in blue, and the voids between the spheres are marked in yellow. (For interpretation of the references to color in this figure legend, the reader is referred to the Web version of this article.)

where $\nu=(1/2\pi) \times (\kappa/\mu)^{1/2}$, n is the vibration quantum number, κ is the force constant, and μ is the reduced mass [24,25].

The $S_0(0)$ rotational mode of para-hydrogen corresponds to the transitions between rotational states with the rotational quantum numbers $J = 0$ and $J = 2$, and its energy is $6B_0$. At the same time, the $S_0(1)$ rotational mode of ortho-hydrogen corresponds to the transitions between rotational states with the rotational quantum numbers $J = 1$ and $J = 3$, and its energy is

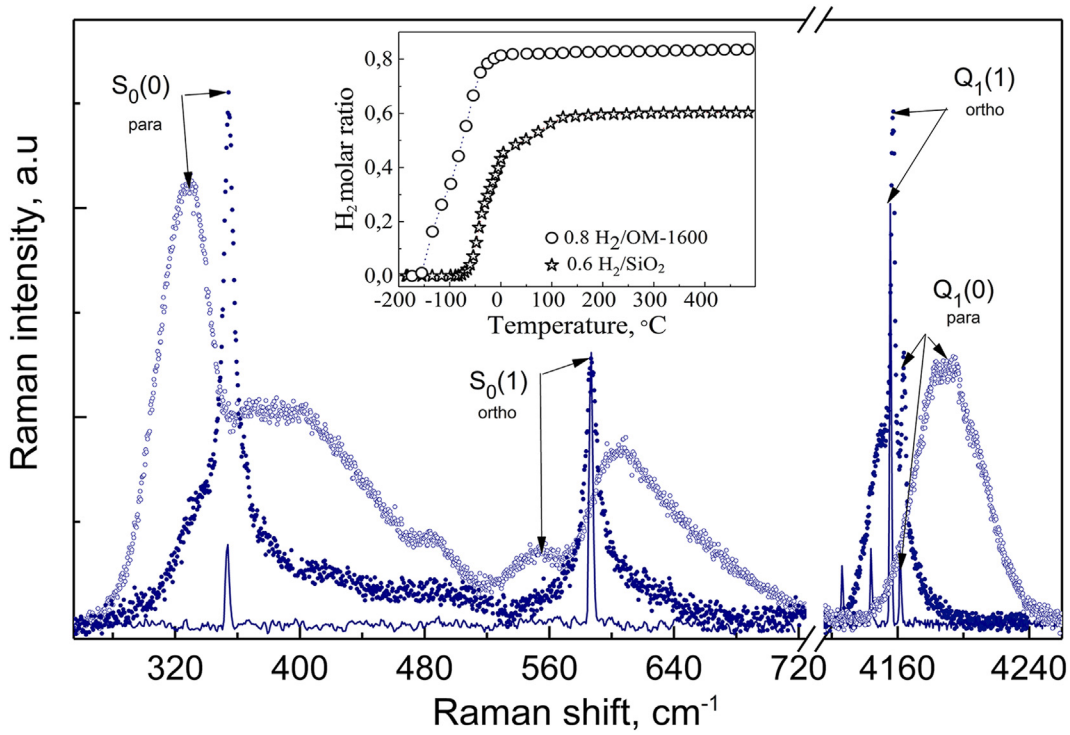

Fig. 2 – Raman spectra of the $0.6H_2/SiO_2$ (open circles) and $0.8H_2$/OM-1600 (solid circles) samples. Solid line: the Raman spectrum of gaseous hydrogen at room temperature and 0.5 MPa. Inset: hot extraction curve of the $0.6H_2/SiO_2$ (stars) and $0.8H_2$/OM-1600 (circles) samples.

$10B_0$. The values of the rotational constant B_0 for gaseous hydrogen under ambient conditions are 59.2 cm^{-1} for the $S_0(0)$ mode and 58.7 cm^{-1} for the $S_0(1)$ mode [26]. Thus, a change in the total nuclear spin of a hydrogen molecule with parallel (ortho, S = 1) and anti-parallel (para, S = 0) nuclear spins of atoms affects the value of the rotational constant B_0 for gaseous hydrogen. The value of the rotational constant changes even more with the enhancement of intermolecular interaction under the transition of hydrogen to a liquid or solid state at a low temperature. For the same reason, the frequencies of the $Q_1(0)$ and $Q_1(1)$ stretching vibration modes of gaseous and liquid hydrogen are also different, and this difference widens at high pressure due to a decrease in the length of the H–H molecular bond.

As shown earlier, the Raman spectrum of hydrogen-saturated silicate glass includes the characteristic phonon modes of amorphous SiO_2, as well as the rotational and stretching vibration modes of molecular hydrogen [12]. As compared to the Raman spectrum of gaseous hydrogen, the phonon modes of hydrogen in silicate glass are strongly broadened and shifted. The rotational modes are shifted to lower energies, their frequencies being about 328 cm^{-1} and 549 cm^{-1}, while the stretching vibration mode is shifted to higher energies, its frequency being about 4190 cm^{-1}. The intensity ratio of two rotational modes of dissolved hydrogen indicates the predominance of para-hydrogen in the hydrogenated silica class at liquid nitrogen temperature as compared to hydrogen gas under ambient conditions. This is related to the ortho-para conversion, which takes place in silica glass hydrides at cryogenic temperatures, just as it occurs in hydrogen liquid and hydrogen clathrate hydrates [24,27]. When hydrogen-saturated samples are heated to room temperature, all phonon modes of hydrogen disappear due to its catastrophic losses, and the Raman spectrum of such samples completely coincides with that of the initial silicate glass [12,28]. Note that the position of the phonon bands of the silicate glass matrix in a hydrogen-saturated sample, as well as the distribution of intensity between them, somewhat differs from the initial one in silicate glass due to the softening of the phonon modes resulting from the expansion of the matrix under hydrogen absorption [12] and the effect of the local van der Waals interaction between silica and hydrogen molecules in the silicate glass voids.

The Raman spectrum of the $0.8H_2$/OM-1600 sample (solid circles) also contains very strong rotational and stretching vibration modes of a hydrogen molecule; their intensity significantly exceeds that of the phonon bands of the initial OM-1600 matrix. It is important to note that in this case, the phonon modes of a hydrogen molecule are represented by two groups of bands, which is well illustrated by the high-frequency vibration mode. This mode consists of a broad band similar to that observed in the Raman spectra of hydrogen-saturated $0.6H_2/SiO_2$ silicate glass and two rather narrow bands close in width to the $Q_1(0)$ and $Q_1(1)$ bands of gaseous hydrogen. The frequency of the narrow bands almost coincides with that of the gaseous hydrogen bands for both the rotational and stretching vibration modes. The broad bands are similar to the phonon modes of dissolved hydrogen in the voids of silica glass, their width being somewhat smaller, and the shift of the rotational and stretching vibration modes being negative and smaller than that in hydrogen-saturated $0.6H_2/SiO_2$ silicate glass. The emergence of two types of hydrogen phonon bands in the Raman spectrum of the $0.8H_2$/OM-1600 samples indicates two different localizations of the absorbed hydrogen molecule: directly in the voids of the amorphous silica spheres and in the mesopores between the silica spheres.

The total amount of absorbed hydrogen in the samples was determined by hot extraction into a pre-evacuated quartz ampoule with a calibrated volume of 50 cm^3 when it was heated to 500 °C at a rate of about ~20 °C/min. The hydrogen hot extraction curve from the $0.6H_2/SiO_2$ samples is shown in the inset in Fig. 2 with stars, while that from the $0.8H_2$/OM-1600 samples is shown with circles. These two curves demonstrate the temperature regions of hydride stability and hydrogen losses in both hydrogenated materials that will be used in further Raman study of hydrogen desorption kinetics during the isothermal annealing of hydrogen-saturated samples. Hydrogen loss from the $0.6H_2/SiO_2$ samples remains insignificant down to −100 °C. With an increase in temperature, it increases markedly and reaches the maximum at ~50 °C. The hydrogen desorption curve for the $0.8H_2$/OM-1600 samples is similar in shape; however, hydrogen losses begin already at −150 °C, and the maximum is reached at about −50 °C. Under heating above ~100 °C, complete release of hydrogen occurs in both cases, the quantitative estimations having shown that the molar ratio $X = H_2/SiO_2$ corresponds to the values of 0.6 and 0.8 for the silicate glass and OM-1600 opal matrices, respectively.

Fig. 3 depicts the Raman spectra of the samples of the initial OM-1600 opal matrix and hydrogen-saturated $0.8H_2$/OM-1600 opal matrices in the energy range of 275–4250 cm^{-1} at ~80 K and ambient pressure (upper part, open and solid circles, respectively). The lower part of Fig. 3 shows the Raman spectra of the samples of initial silicate glass and the hydrogen-saturated $0.6H_2/SiO_2$ sample under the same conditions (open and solid circles, respectively). The Raman spectra of the samples of initial opal matrices and silicate glass are rather similar and differ in some details only. The phonon bands of the initial OM-1600 opal matrix are slightly shifted towards higher energies and broadened, which may be due to internal stresses in the primary silica microspheres resulting from their small sizes. At the same time, the Raman spectra of the hydrogen-saturated samples differ quite strongly: the rotational and stretching vibration phonon modes of a hydrogen molecule in the $0.8H_2$/OM-1600 sample are represented by two groups of bands. This is clearly seen in the inset in Fig. 3, which highlights the stretching vibration mode and shows its decomposition into individual bands. The broad band in the decomposition resembles the stretching vibration mode in the hydrogen-saturated $0.6H_2/SiO_2$ silica glass in terms of shape and width. Two narrow bands with a frequency of 4163.7 and 4157 cm^{-1}, the width of which is an order of magnitude smaller than that of the broad band, almost coincide in frequency with the $Q_1(0)$ and $Q_1(1)$ modes of hydrogen in the gas phase (4162.5 and 4155.5 cm^{-1}). The small difference between them may be related to different temperatures of measurements: in the hydrogen-saturated opal matrices, they were carried out at liquid nitrogen temperature, and the frequencies are slightly higher.

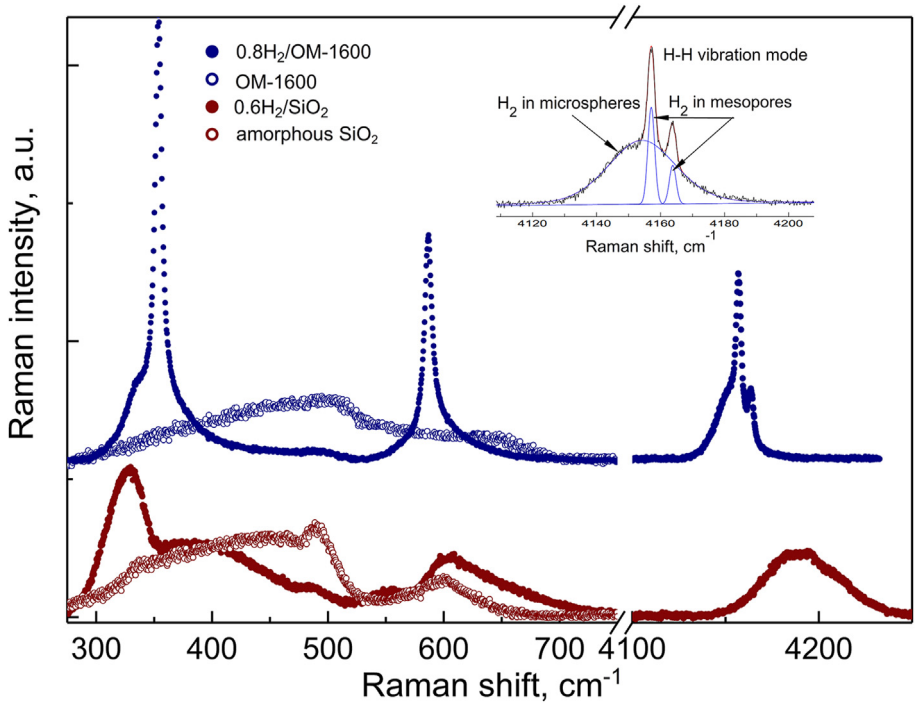

Fig. 3 – Bottom: Raman spectra of the $0.6H_2/SiO_2$ silica glass hydride (solid circles) and initial quartz glass (open circles). Top: Raman spectra of the $0.8H_2$/OM-1600 sample (solid circles) and the OM-1600 opal matrix (open circles). Inset: decomposition of the vibration band in the Raman spectrum of the $0.8H_2$/OM-1600 sample into individual bands.

The width of the stretching vibration modes and the proximity of their frequencies in the Raman spectra of the $0.8H_2$/OM-1600 sample to those of the stretching vibration mode of gaseous hydrogen indicate that they are most likely related to the hydrogen molecules located inside the relatively large mesopores between the "secondary" silica spheres. At the same time, the broad band is associated with the hydrogen molecules located directly inside the highly small voids in the amorphous silica microspheres and dense concentric amorphous silica shells. The same picture is seen also for the rotational modes: in the Raman spectrum of the $0.8H_2$/OM-1600 sample, they are also represented by narrow and wide bands, as indicated by a wide shoulder near the lowest $S_0(0)$ rotational mode. Thus, in the $0.8H_2$/OM-1600 sample, the molecules of adsorbed hydrogen have two different localizations: directly in the "primary" silica microspheres and in the mesopores between the "secondary" silica spheres.

The hot extraction data show the total losses of hydrogen from two different locations in the $0.8H_2$/OM-1600 sample that begin at −150 °C and increase with a further increase in temperature. However, the question is whether these losses occur in a parallel way from both locations or preferably from one of them. This issue requires special study: at first glance, the losses of hydrogen from the mesopores between the secondary particles can outstrip other losses. The exact answer can be received by investigating changes in the Raman intensities of broad and narrow bands of the $0.8H_2$/OM-1600 sample *in-situ* under isothermal heating, which should show the loss of hydrogen from both locations. The left side of Fig. 4 demonstrates the Raman spectra of the hydrogen-saturated $0.8H_2$/OM-1600 sample in the vibration mode region in the energy range of 4100–4200 cm^{-1} at heating times of 4, 7, 13, and 22 min and a temperature of 185 K. The background signal, which is most likely related to the luminescence of the defects formed during hydrogen absorption at high pressure and temperature, was subtracted from these spectra. The intensity of the spectrum was preliminarily normalized by the magnitude of the background luminescence signal at a frequency of 4000 cm^{-1} outside the region of vibration bands in the Raman spectrum. That reduced the systematic measurement error associated with possible deviation from the initial focusing of the laser in the excitation spot on the sample surface. The total intensity of the vibration band in the Raman spectrum gradually decreased with an increase in the annealing time due to increasing losses of dissolved hydrogen. The dependence of the integral intensity of the H–H stretching vibration mode on the annealing time is shown in the upper inset in Fig. 4. It demonstrates an exponential decrease in the total amount of absorbed hydrogen with annealing time, reaching saturation about 30 min after the annealing onset (open circles, left scale). Note that hydrogen desorption in the hydrogenated silica glass is of activation nature, and the attainment of saturation is related to the peculiarities of the Raman measurements in back-scattering geometry, in which a signal is recorded from the subsurface region of the samples. As we have shown earlier, saturation is associated with the delayed diffusion of hydrogen from the sample depth [14]. The solid circles in the inset in Fig. 4 indicate the time dependence of the relative fraction of hydrogen absorbed by the primary silica spheres to the total amount of absorbed hydrogen in two localizations (right scale). This ratio was calculated by decomposing the experimental Raman spectrum into

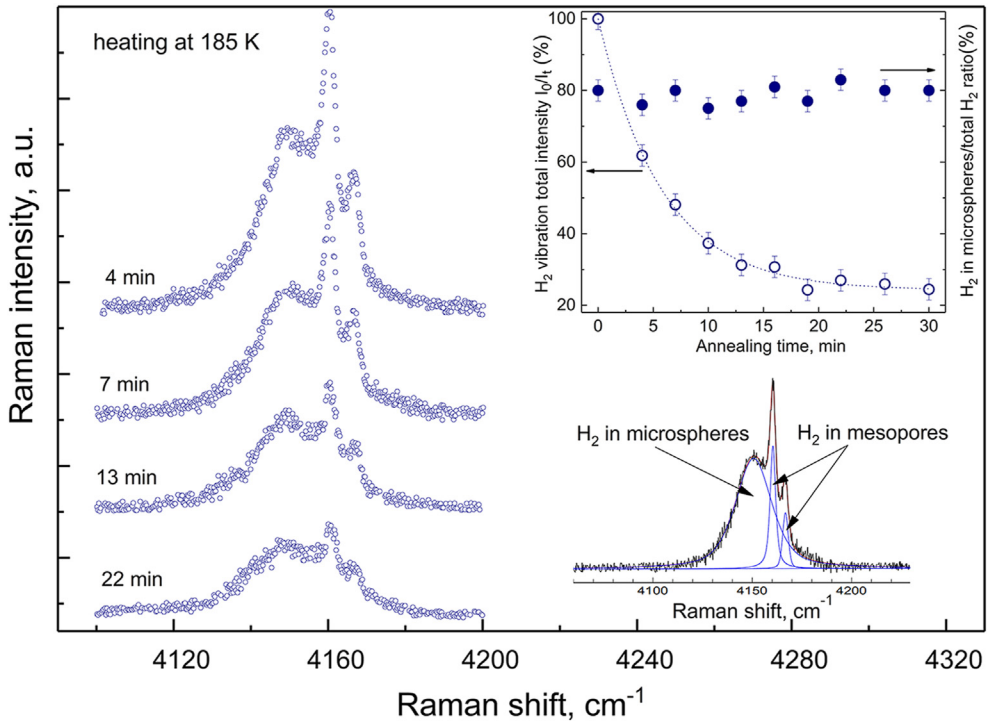

Fig. 4 – Raman spectra of the 0.8H_2/OM-1600 sample in the vibration mode region after 4, 7, 13, and 22 min of annealing at 185 K (left). Inset on the top right side: dependence of the total intensity of the vibration band on the annealing time (open circles) and its approximation by the exponential decay function (dashed line). Solid circles: dependence of the relative intensity of the hydrogen band inside the silica microspheres to the total intensity of the vibration mode. Inset on the bottom right side: an example of the decomposition of the vibration mode into individual components.

individual bands (lower inset in Fig. 4), which was used to determine the integral intensities of the vibration bands of hydrogen in two localizations. The resulting value is almost independent of the annealing time and is on average (79 ± 2) %. Thus, under the heating of hydrogen-saturated opal matrices, hydrogen losses occur with the same intensity from the voids in the amorphous silica spheres and the mesopores between them.

The hydrogen losses during the annealing of the 0.8H_2/OM-1600 sample lead to a gradual decrease in the intensity of the hydrogen rotational modes in the Raman spectrum. These changes can be quantified by the ratio of the integral intensity of the rotational modes to the total intensity of the phonon modes of the initial OM-1600 sample. The latter is insensitive to annealing and does not change with temperature, so it can be used to calibrate the intensity scale. The right inset in Fig. 5 shows the evolution of the Raman spectra of the 0.8H_2/OM-1600 sample in the frequency range of 300–700 cm^{-1} during its annealing at a fixed temperature of 183 K for 3, 11, 15, and 28 min. The upper part of the inset illustrates the decomposition of the spectrum into individual bands by the fitting of their profile using the Voigt function. The spectrum includes wide and narrow bands related to the rotational modes of hydrogen inside the voids of the primary silica microspheres and the mesopores between them, respectively, as well as very broad bands associated with the phonon modes of amorphous silica. As can be seen from the spectra above, the intensity of the rotational modes decreases consistently with an increase in the isothermal heating time. On the left side of Fig. 5, the circles mark the ratio of the integral intensity of the rotational modes of hydrogen to the total intensity of the phonon modes of the OM-1600 opal matrix depending on the annealing time at three different temperatures. The dashed line shows the fitting of the experimental data by the exponential decay function, the initial value at all temperatures being normalized to unity. This dependence reflects an exponential decrease in the hydrogen content in the 0.8H_2/OM-1600 sample during annealing and is well described by the function $I_{H2}/I_{SiO2} = A*\exp(-t/\tau)+B$. Here, τ is the time constant of the exponential decay that varies from 48 min at 163 K to 2.2 min at 213 K. The exponential dependence of the hydrogen content on the annealing time and a decrease in the time constant of exponential decay with an increase in the annealing temperature indicate the activation nature of hydrogen desorption in the 0.8H_2/OM-1600 samples. Under these conditions, hydrogen content should tend to zero at a long heating time due to the complete depletion of hydrogen in the subsurface layer. This is related to the peculiarities of the Raman measurements in back-scattering geometry, in which a signal is recorded from the subsurface region of the samples. Nevertheless, the exponential decay curve attains saturation at some non-zero level that decreases with an increase in the annealing temperature. Note that slow diffusion of hydrogen from the depth of the sample to its surface results in the partial replenishment of released hydrogen in the subsurface layer. The hydrogen desorption rate decreases at

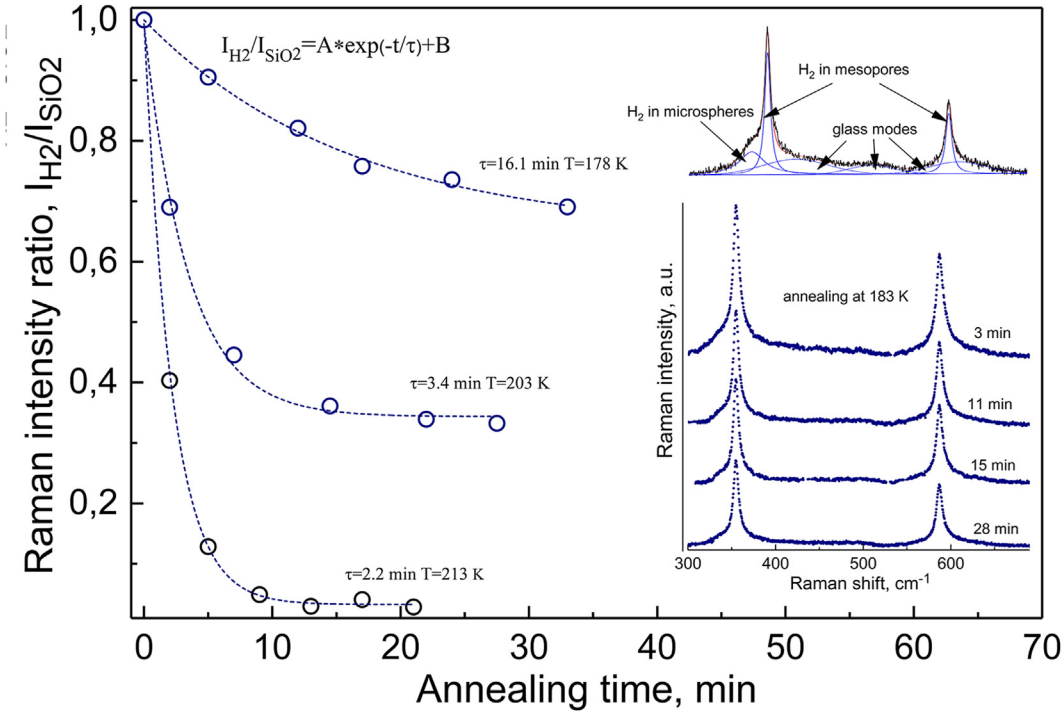

Fig. 5 – Dependence of the relative intensity I_{H2}/I_{SiO2} of the rotational hydrogen modes to the intensity of the phonon modes of the OM-1600 opal matrix on the annealing time at 178, 203, and 213 K (open circles). Dashed line: approximation by the exponential decay function. Inset: Raman spectra of the 0.8H_2/OM-1600 sample for various times of annealing at 183 K. Top: an example of the decomposition of the Raman spectrum into individual components.

longer annealing times and equalizes at a certain moment with an initially lower diffusion rate, at which the exponential decay curve attains saturation. At higher annealing temperatures, hydrogen desorption increases faster than hydrogen diffusion, and saturation occurs at shorter annealing times and lower hydrogen content. This situation can arise if the activation energy of diffusion is higher than that of hydrogen desorption.

The obtained experimental data show that hydrogen desorption in the 0.8H_2/OM-1600 samples sharply enhances with an increase in temperature. The measurements of the Raman spectra within the available temperature range demonstrate that the time constant of the exponential decay τ decreases from ~2860 s at a minimum annealing temperature of 163 K to ~130 s at a maximum temperature of 213 K. Hydrogen desorption undoubtedly is of activation nature and can be described by the Arrhenius equation:

$$\tau(T) = A \times \exp(E_A/k_B T) \quad (3)$$

where τ is the time constant of the exponential decay, T is the temperature, E_A is the activation energy, k_B is the Boltzmann constant, and A is the coefficient preceding the exponent with the dimension of time. In Fig. 6, open circles show the experimental data on the dependence of the time constant of the exponential decay τ (the Y axis, logarithmic scale) on the reciprocal temperature $1/k_BT$ (the X axis, linear scale), and the dashed line is their linear approximation in accordance with Eq. (3); at that, the activation energy E_A is (162 ± 13) meV, and the time constant A is (1.8 ± 0.5) × 10^{-2} s. These values are very close to those obtained earlier for hydrogen-saturated silicate glass, which are E_A=(160 ± 10) meV and

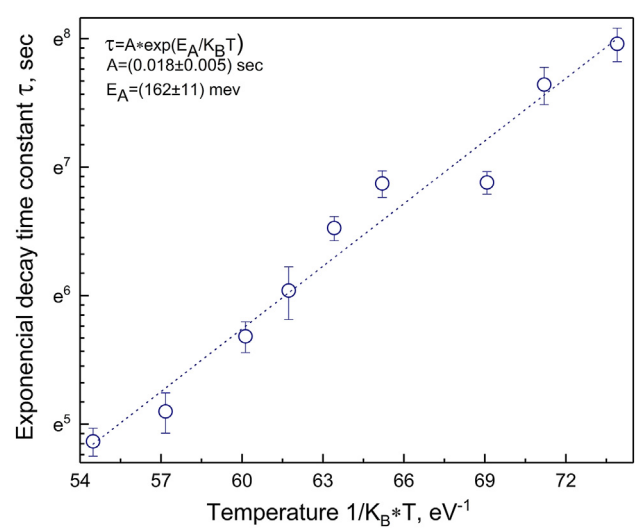

Fig. 6 – Arrhenius dependence $\tau(T) = A \times \exp(E_A/k_BT)$ of the time constant of the exponential decay τ on the annealing temperature $1/k_BT$ (open circles) and its approximation by the linear function (dashed line). E_A is the activation energy, A is the time constant, and k_B is the Boltzmann constant.

$A = (2.7 \pm 0.3) \times 10^{-2}$ s [14]. The proximity of these data is primarily due to the significant predominance of hydrogen localized in the amorphous silica microspheres over hydrogen localized in the mesopores between them. Moreover, the retention of hydrogen in both localizations is of common nature and results from the weak van der Waals interaction between the molecules of hydrogen H_2 and silica SiO_2, which causes low activation energy of hydrogen desorption. In light of this, it is interesting to compare the obtained results for the activation energy of hydrogen desorption in hydrogenated silica glass and opal matrices with those of classical lithium and magnesium hydrides as LiH and MgH_2 with ionic and covalent chemical bonds [1,29,30]. The activation energy of hydrogen desorption of 181 kJ/mol in the LiH hydride is about 12 times higher than the activation energy of hydrogen desorption of 0.16 eV/particle (equivalent to 15.5 kJ/mol H_2) in hydrogenated silica glass [29]. The magnesium MgH_2 hydride is characterized by the activation energy of hydrogen desorption of 174 kJ/mol, which is close to that of the lithium hydride [1,30]. MgH_2 doped with 5 wt% of vanadium leads to a decrease in the activation energy of hydrogen desorption to 119 kJ/mol, while doping with 5 wt% of nickel results in even less activation energy of a 75 kJ/mol [31]. The improved hydrogen storage parameters have been obtained recently for Mg–Nb@C nanocomposite, which shows better parameters of dehydrogenation and its activation energy of 59.7 kJ/mol [32,33]. Note that the hydrogen storage conditions for silica glass and synthetic opal matrices considerably differ from those of pure and doped magnesium hydrides. For the latter materials, the hydrogenation/dehydrogenation temperature, the activation energy of hydrogen desorption, and hydrogen capability are higher, while the hydrogen gas pressure is lower.

Finally, it seems to be interesting to compare the activation energy of hydrogen desorption with that of hydrogen diffusion in silicate glass to verify the proposed saturation mechanism of the exponential decay curve. As was shown earlier, silicate glass is quite permeable to hydrogen, and the diffusion of hydrogen in it increases with an increase in temperature, demonstrating activation behavior [34–36]. The penetration of hydrogen through a bridge in a quartz ampoule separating one half of it with hydrogen gas from the other half with carbon dioxide was studied by the Raman scattering method. The amount of hydrogen that passed through the bridge between the ampoules was determined from the relative intensity of the hydrogen stretching vibration mode in the Raman spectrum of the ampoule initially filled with pure carbon dioxide. The activation energy of hydrogen diffusion determined in these experiments varied from 0.37 eV to 0.43 eV in early publications [34,35]. In the later work, the value of 0.54 eV was given [36]. Thus, the activation energy of hydrogen diffusion in silicate glass is at least two and a half times higher than that of hydrogen desorption in hydrogenated silicate glasses and synthetic opal matrices. Thereby, in the temperature range under study, the diffusion of hydrogen from the depth of the samples to their surface occurs relatively slower than hydrogen desorption from the subsurface layer. This permits dividing the processes of desorption and diffusion since hydrogen losses proceed at an outstripping rate due to desorption and are not fully compensated by the diffusion of hydrogen from the sample depth.

Conclusions

In opal matrices of silica microspheres with a diameter of 0.235 μm and 1.6 μm, the effective absorption of molecular hydrogen occurs at P = 7.5 GPa and T = 140 °C, reaching the maximum value of the molar ratio $X = H_2/SiO_2$ of 0.8. In the Raman spectra of the hydrogen-saturated opal matrices formed by silica microspheres with a diameter of 0.235 μm and 1.6 μm, absorbed hydrogen is represented by two groups of bands: wide and narrow bands of the rotational and stretching vibration modes corresponding to two different localizations of a hydrogen molecule in the matrix. The narrow bands are close in width and frequency to the corresponding bands of gaseous hydrogen at low pressure [3]. They are most likely related to the embedding of hydrogen into the mesopores between the silica spheres of the opal matrix, and their frequency and width indicate that hydrogen molecules weakly interact with each other, as is the case in a gas. Hydrogen molecules are held inside the mesopores and silica spheres by the van der Waals interaction with SiO_2 molecules. The broad bands are similar to the analogous bands of a hydrogen molecule in the Raman spectra of silicate glass with absorbed hydrogen [12]. The width of these bands in the hydrogenated opal matrices is somewhat smaller than that in the hydrogen-saturated samples of silicate glass. At the same time, the frequency of the rotational mode is somewhat higher, and the frequency of the stretching vibration mode is somewhat lower. These bands are associated with hydrogen molecules embedded into the pores of the "primary" silica spheres and dense concentric silica shells inside structural units of the opal matrices. In contrast to the samples of silicate glass, in OM-1600 there are mesopores between the silica spheres, and their filling with hydrogen leads to a decrease in the hydrogen absorption directly in the voids of the "primary" silica microspheres. In our view, significant differences between the sizes of the voids in silicate glass and those of the pores between the silica spheres are the main reason for the marked differences in the width and position of the rotational and stretching vibration modes of the hydrogen molecules in two different localizations. To a certain extent, this situation is similar to the absorption of hydrogen at cryogenic temperatures in porous quartz Vycor glasses containing a significant number of cylindrical void channels with a diameter up to 12 nm [37]. In this work, some difference in the width and frequency of the rotational and stretching vibration bands in the Raman spectra was also observed for hydrogen absorbed in a silicate glass array and cylindrical channels.

The hydrogen-saturated OM-1600 samples are unstable at a high temperature and intensively release hydrogen under heating. Their annealing at temperatures in the range of 163–213 K leads to an exponential drop in the hydrogen content, with the time constant of the exponential decay decreasing dramatically. The dependence of the time constant of the exponential decay τ on the reciprocal temperature $1/k_BT$ is well described by the Arrhenius equation, and the

activation energy E_A and the time constant A are (162 ± 13) meV and (1.8 ± 0.5) × 10^{-2} s, respectively. These values are close to those obtained earlier for silicate glass filled with hydrogen. By using Eq. (3), the stability of the $0.8H_2$/OM-1600 samples can be estimated as follows: the hydrogen content in them will be reduced by half in about 16 years when stored in liquid nitrogen, and at room temperature this will happen in about 5 s. The obtained data coincide within the experimental error with similar values for silicate glass with absorbed hydrogen obtained earlier in Ref. [14].

This work was carried out within the state task of ISSP RAS.

Declaration of competing interest

The authors declare that they have no known competing financial interests or personal relationships that could have appeared to influence the work reported in this paper.

REFERENCES

[1] Yartys VA, Lototskyy MV, Akiba E, Albert R, Antonov VE, Ares JR, Baricco M, Bourgeois N, Buckley CE, et al. Magnesium based materials for hydrogen based energy storage: past, present and future. Int J Hydrogen Energy 2019;44:7809–59. https://doi.org/10.1016/j.ijhhydene.2018.12.212.

[2] Timothy A, Strobel TA, Sloan ED, Koh CA, Huq A, Schultz AJ. Molecular hydrogen occupancy in binary THF–H2 clathrate hydrates by high resolution neutron diffraction. J Phys Chem B 2006;110(29):14024–7. https://doi.org/10.1021/jp063164w.

[3] Meletov KP, Maksimov AA, Tartakovskii II, Bashkin IO, Shestakov VV, Krestinin AV, YuM Shulga, Andrikopoulos K, Arvanitidis Y, Christifilos D, Kourouklis GA. Raman study of the high-pressure hydrogenated SWNT: in search of chemically bonded and adsorbed molecular hydrogen. Chem Phys Lett 2007;433:335–9. https://doi.org/10.1016/j.cplett.2006.11.072.

[4] Lokshin KA, Zhao Yusheng. Fast synthesis method and phase diagram of hydrogen clathrate hydrate. Appl Phys Lett 2006;88:131909. https://doi.org/10.1063/1.2190273.

[5] Efimchenko VS, Fedotov VK, Kuzovnikov MA, Zhuravlev AS, Bulychev BM. Hydrogen solubility in amorphous silica at pressures up to 75 kbar. J Phys Chem B 2013;117:422–5. https://doi.org/10.1021/jp309991x.

[6] Durbin DJ, Malardier-Jugroot C. Review of hydrogen storage techniques for on board vehicle applications. Int J Hydrogen Energy 2013;38:14595–617. https://doi.org/10.1016/j.ijhhydene.2013.07.-58.

[7] Jena P. Materials for hydrogen storage: past, present, and future. J Phys Chem Lett 2011;2:206–11. https://doi.org/10.1021/jz1015372.

[8] Efimchenko VS, Fedotov VK, Kuzovnikov MA, Meletov KP, Bulychev BM. Hydrogen solubility in cristobalite at high pressure. J Phys Chem A 2014;118:10268–72. https://doi.org/10.1021/jp509470q.

[9] Efimchenko VS, Barkovskii NV, Fedotov VK, Meletov KP, Simonov SV, Khasanov SS, Khryapin KI. High-pressure solid solutions of molecular hydrogen in amorphous magnesium silicates. J Alloys Compd 2019;770:229–35. https://doi.org/10.1016/j.jallcom.2018.08.111.

[10] Schmitt ML, Shelby JE, Hall MM. Preparation of hollow glass microspheres from sol–gel derived glass for application in hydrogen gas storage. J Non-Cryst Solids 2006;352:626–31. https://doi.org/10.1016/j.jnoncrysol.2005.11.057.

[11] Kucheyev SO, Van Cleve E, Worsley MA. Freezing and melting of hydrogen confined in nanoporous silica. J Phys Condens Matter 2014;26:225004. https://doi.org/10.1088/0953-8984/26/22/225004.

[12] Meletov KP, Efimchenko VS. Raman study of hydrogen-saturated silica glass. Int J Hydrogen Energy 2021;46:24501–9. https://doi.org/10.1016/j.ijhhydene.2021.04.144.

[13] Bashkin IO, Antonov VE, Bazhenov AV, Bdikin IA, Borisenko DN, et al. Thermally stable hydrogen compounds obtained under high pressure on the basis of carbon nanotubes and nanofibers. JETP Lett 2004;79:226–30. https://doi.org/10.1134/1.1753421.

[14] Meletov KP, Efimchenko VS. Stability of hydrogenated silica glass and desorption kinetics of molecular hydrogen. Chem Phys Lett 2022;793:139477. https://doi.org/10.1016/cplett.2022.139477.

[15] Stöber W, Fink A, Bohn E. Controlled growth of monodisperse silica spheres in the micron size range. J Colloid Interface Sci 1968;26:62–9. https://doi.org/10.1016/0021-9797(68)90272-5.

[16] Samarov EN, Mokrushin AD, Masalov MV, Abrosimova GE. Emel'chenko GA Structural modification of synthetic opals during thermal treatment. Phys Solid State 2006;48:1280–3. https://doi.org/10.1134/S1063783406070109.

[17] Masalov VM, Sukhinina NS, Kudrenko EA, Emelchenko GA. Mechanism of formation and nanostructure of Stöber silica particles. Nanotechnology 2011;22:275718. https://doi.org/10.1088/0957-4484/22/27/275718.

[18] Masalov VM, Kudrenko EA, Grigoryeva NA, Ezdakova RV, Roddatis VV, Sukhinina NS, Arefev MV, Mistonov AA, Grigoriev SV, Emelchenko GA. Direct observation of the shell-like structure of SiO_2 particles synthesized by the multistage Stöber method. Nano 2013;8:1350036. https://doi.org/10.1142/S1793292013500367.

[19] Bardyshev AD, Mokrushin AA Pribylov, Samarov EN, Masalov VM, Karpov IA, Emelchenko GA. Porous structure of synthetic opals. Colloid J 2006;68:20–5. https://doi.org/10.1134/S1061933X06010029.

[20] Khvostantsev LG, Slesarev VN, Brazhkin VV. Toroid type high-pressure device: history and prospects. High Pres Res 2004;24:371–83. https://doi.org/10.1080/08957950412331298761.

[21] Antonov VE, Bashkin IO, Khasanov SS, Moravsky AP, Morozov YuG, YuM Shulga, Ossipyan YuA, Ponyatovsky EG. Magnetic ordering in hydrofullerite $C_{60}H_{24}$. J Alloys Compd 2002;330–332:365–8. https://doi.org/10.1016/S0925-8388(01)01534-1.

[22] Antonov VE, Bulychev BM, Fedotov VK, Kapustin DI, Kulakov VI, Sholin IA. NH_3BH_3 as an internal hydrogen source for high pressure experiments. Int J Hydrogen Energy 2017;42:22454–9. https://doi.org/10.1016/j.ijhydene.2017.03.121.

[23] Meletov KP. A nitrogen cryostat with adjustable temperature and cold loading of samples for the measurement of optical spectra. Instrum Exp Tech 2020;63:291–3. https://doi.org/10.1134/S0020441220020013.

[24] McLennan JC, McLeod JH. The Raman effect with liquid oxygen, nitrogen, and hydrogen. Nature 1929;123:160. https://doi.org/10.1038/123160a0.

[25] Landau LD, Lifshitz EM. Quantum mechanics: non-relativistic theory. 3rd ed. New York: Pergamon; 1977. Chapter11.

[26] Allin EJ, Feldman T, Welsh HL. Raman spectra of liquid and solid hydrogen. J Chem Phys 1956;24:1116–7. https://doi.org/10.1063/1.1742711.

[27] Strobel TA, Sloan ED, Koh CA. Raman spectroscopic studies of hydrogen clathrate hydrates. J Chem Phys 2009;130:014506. https://doi.org/10.1063/1.3046678.

[28] Chrissanthopoulos A, Bouropoulos N, Yannopoulos SN. Vibrational spectroscopic and computational studies of sol-gel derived CaO-MgO-SiO_2 binary and ternary bioactive glasses. Vib Spectrosc 2008;48:118–25. https://doi.org/10.1016/j.vibspec.2007.11.008.
[29] Jain A, Miyaoka H, Ishikava T. Destabilization of lithium hydride by the substitution of group 14 elements: a review. Int J Hydrogen Energy 2010;35:5133–44. https://doi.org/10.1016/ijhydene.2016.02.060.
[30] Jain I, Lal C, Jain A. Hydrogen storage in Mg: a most promising material. Int J Hydrogen Energy 2016;41:5969–78. https://doi.org/10.1016/ijhydene.2009.08.88.
[31] Sakintuna B, Lamaridarkrim Hirsher M. Metal hydride materials for solid hydrogen storage: a review. Int J Hydrogen Energy 2007;32:1121–40. https://doi.org/10.1016/ijhydene.2006.11.022.
[32] Zhu C, Chen M, Hu M, He D, Liu Y, Liu T. Hydrogen storage properties of Mg-Nb@C nanocomposite: effects of Nb nanocatalyst and carbon nanoconfinement. Int J Hydrogen Energy 2021;46:9443–510. https://doi.org/10.1016/ijhydene.2020.12.099.
[33] Zheng J, Wang CG, Zhou H, Ye E, Xu J, Li Z, Loh XJ. Current research trends and perspectives on solid-state nanomaterials in hydrogen storage. Resarch 2021. https://doi.org/10.34133/2021/375089. ID 3750689.
[34] Lee RW, Frank RC, Swets DE. Diffusion of hydrogen and deuterium in fused quartz. J Chem Phys 1962;36:1062–70. https://doi.org/10.1063/1.1732632.
[35] Shelby JE. Molecular diffusion and solubility of hydrogen isotopes in vitreous silica. J Appl Phys 1977;48:3387–94. https://doi.org/10.1063/1.324180.
[36] Shang L, Chou I-M, La W, Burruss RC, Zhang Y. Determination of diffusion coefficients of hydrogen in fused silica between 296 and 523 K by Raman spectroscopy and application of fused silica capillaries in studying redox reactions. Geochem Cosmochim Acta 2009;73:5435–43. https://doi.org/10.1016/j.gca.2009.0.
[37] De Kinder J, Bouwen A, Schoemaker D. Molecular hydrogen in porous Vycor glass. Phys Rev B 1995;52:15872–80. https://doi.org/10.1103/PhysRevB.52.15872.